First satellite-imaging observation of medium-scale traveling ionospheric disturbances by FORMOSAT-2/ISUAL

Toru Adachi,[1,2] Yuichi Otsuka,[3] Masashi Yamaoka,[1] Mamoru Yamamoto,[1] Kazuo Shiokawa,[3] Alfred B. Chen,[4] and Rue-Ron Hsu[5]

Received 22 November 2010; revised 13 January 2011; accepted 18 January 2011; published 16 February 2011.

[1] On the night of May 16, 2007, a satellite limb imager of FORMOSAT-2/ISUAL observed wave-like structures of the 630-nm airglow simultaneously with an all-sky imager deployed at Darwin in Australia. The height of the airglow layer was estimated as 220 km, and the structures were aligned in the northeast-southwest orientation with a wavelength of ~300 km and propagated toward the northwest with a phase velocity of ~100 m s^{-1}, showing typical characteristics of the nighttime medium-scale traveling ionospheric disturbances (MSTIDs). We conclude that ISUAL for the first time succeeded in observing the airglow layer altitude and airglow structures modulated by MSTID from space. Such a satellite limb airglow imaging could be a new tool to characterize ionospheric irregularities on a global level. **Citation:** Adachi, T., Y. Otsuka, M. Yamaoka, M. Yamamoto, K. Shiokawa, A. B. Chen, and R.-R. Hsu (2011), First satellite-imaging observation of medium-scale traveling ionospheric disturbances by FORMOSAT-2/ISUAL, *Geophys. Res. Lett.*, *38*, L04101, doi:10.1029/2010GL046268.

1. Introduction

[2] Nighttime medium-scale traveling ionospheric disturbances (MSTIDs) at midlatitudes are banded structures of the ionosphere with a wavelength of 50–500 km and propagate with a phase velocity of 50–170 m s^{-1} [*Garcia et al.*, 2000]. They are typically elongated in the northwest-southeast (northeast-southwest) direction and propagate toward the southwest (northwest) in the Northern (Southern) Hemisphere [*Otsuka et al.*, 2004]. Past ground-based all-sky imagers [e.g., *Garcia et al.*, 2000; *Otsuka et al.*, 2004] and GPS-TEC radio measurements [e.g., *Saito et al.*, 2001] extensively clarified their spatiotemporal characteristics.

[3] Linear theory of the Perkins instability [*Perkins*, 1973] well explains the orientation of the banded structures of MSTIDs but does not fully satisfy the observed features in terms of propagation direction and growth rate. Recent studies suggested that irregularities occurring in the F-region ionosphere are coupled with those in the E-region [e.g., *Cosgrove and Tsunoda*, 2004; *Otsuka et al.*, 2007] and in the conjugate hemisphere [*Otsuka et al.*, 2004]. These findings indicated a strong need to study the non-linear behavior of MSTIDs in a larger spatial scale, and satellite-based global measurements would be one of the most important methods for this purpose. While several studies clarified electric/magnetic field fluctuations associated with MSTIDs using satellite observations [e.g., *Saito et al.*, 1995; *Park et al.*, 2009], space-borne imaging techniques have never been utilized. This paper for the first time reports a successful imaging observation of an MSTID event from space.

2. Observation and Results

[4] The Imager for Sprites and Upper Atmospheric Lightning (ISUAL) payload on the FORMOSAT-2 satellite consists of an imager with a selectable six-color filter wheel, a six-color spectrophotometer, and a dual-color array photometer, with all fields-of-view (FOV) directed toward the midnight (0LT) limb [*Adachi et al.*, 2010]. The primary targets of ISUAL are lightning and transient luminous events (TLEs) [e.g., *Adachi et al.*, 2008] and, therefore, airglow observations described in the present paper were carried out on a special request basis. The data analyzed were obtained by the ISUAL imager with a 628–635 nm filter which is designed to observe the atomic oxygen emission at 630 nm. The imager covers an area of ~980 km (horizontal) × ~240 km (vertical) at a spatial resolution of ~1.9 km at the limb located ~2800 km away from the satellite. Taking images at a repetition rate of ~20 s^{-1} as the satellite moves northward on the orbit, ISUAL scanned airglow structures between ~50°S and ~25°N in the northern winter seasons and between ~40°S and ~35°N in the equinox seasons. From these data, *Adachi et al.* [2010] determined the height of the 630-nm airglow layer and showed the latitudinal distribution of the layer. The latitudinal distribution of the airglow layer has also been surveyed by several other limb measurements [e.g., *Zhang and Shepherd*, 2008]. The present paper, on the other hand, focuses on the data of medium-scale (several hundred kilometers) airglow structures observed over Darwin in Australia on the night of May 16, 2007. Figure 1a shows a limb image of the 630-nm airglow over Darwin at 1459:54 UT. Lower bright emissions are due to the OH airglow layer whereas upper dim emissions are due to the OI (630-nm) airglow layer. Figures 1b–1d show perturbations of the 630-nm airglow successively observed at around 1500 UT. The perturbation component was derived by subtracting, on a pixel-by-pixel basis, the mean airglow data obtained along the satellite orbit from ~53°S to ~31°N. Several characteristic structures can be

[1] Research Institute for Sustainable Humanosphere, Kyoto University, Uji, Japan.
[2] Department of Electrical Engineering, Stanford University, Stanford, California, USA.
[3] Solar-Terrestrial Environment Laboratory, Nagoya University, Nagoya, Japan.
[4] Institute of Space, Astrophysical and Plasma Sciences, National Cheng Kung University, Tainan, Taiwan.
[5] Department of Physics, National Cheng Kung University, Tainan, Taiwan.

0094-8276/11/2010GL046268

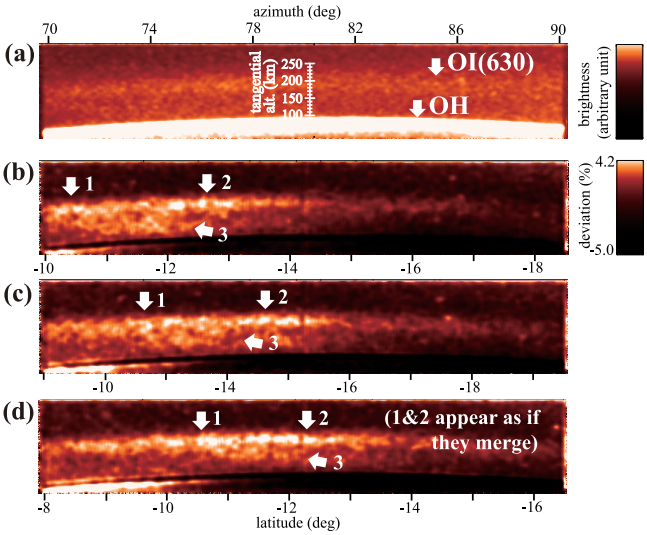

Figure 1. (a) Limb image obtained by FORMOSAT-2/ISUAL over Darwin at 1459:54 UT on May 16, 2007. Lower bright emissions are due to the OH airglow layer while upper dim emissions are due to the OI (630-nm) airglow layer. Note that the true height of the 630-nm airglow layer is typically 20–30 km higher than the tangential altitude shown here [*Adachi et al.*, 2010]. (b–d) Deviations of the airglow successively obtained with a time interval of ~20 seconds at around 1500 UT.

found in Figures 1b–1d. The arrows 1 and 2 indicate two bright regions in the limb airglow layer while the arrow 3 indicates another structure which was probably located on the curved horizontal plane and was extended toward the observer from the limb enhancement 1. Note that the signal level of these structures is only ~1 sigma deviation in a single image. However, because they are consistently observed at nearly the same geographical locations in five successive images (three of them are shown), statistical confidence level is 97–99%. We conclude therefore that these structures are not due to instrument noise or analysis errors, but to true phenomena. The distance between structures 1 and 2 in Figure 1b was estimated as several hundred kilometers, which is comparable with MSTIDs. Interestingly, the structures in Figure 1d are ambiguous and even appear as if they merge. If they are due to MSTIDs typically oriented in the northeast-southwest direction in the Southern Hemisphere, ISUAL can more clearly identify them in the left side of FOV (directed toward 20° north of east) rather than in the right side (east), since the line-of-sight is more closely aligned with the orientation of MSTIDs at the left edge (Figure 3a). Thus, this feature suggests that they are due to northeast-southwest oriented structures such as MSTIDs.

[5] An all-sky airglow imager has been in operation at Darwin (12.4°S, 131.0°E; magnetic latitude 22°S) in Australia since October 2001 as part of the Optical Mesosphere Thermosphere Imagers (OMTIs) [*Shiokawa et al.*, 2009]. The imager has five optical filters, a fish-eye lens with a field-of-view of 180°, and a cooled-CCD camera with 512 × 512 pixels. The imager is calibrated using a 2-m integrating sphere in order to determine the absolute intensity in Rayleigh units [*Shiokawa et al.*, 2000]. Two-dimensional images of OI (630.0 nm) airglow intensity were obtained every 330 s with exposure times of 165 s. Figure 2a shows a map of the 630-nm airglow intensity observed at Darwin 1502 UT on May 16, 2007. Because the difference in observation time between the ISUAL and all-sky imager data was only ~2 minutes, it is possible to say both instruments simultaneously observed spatiotemporal structures of the same MSTID from space and ground. Based on the true height of the layer (220 km) estimated by the ISUAL limb image, the all-sky image from the ground was converted into the geographical coordinates. The color scale in the map shows percentage of the airglow intensity perturbation to the background intensity. The perturbation component was obtained from deviation from the 1-hour average of the airglow intensity. MSTIDs can be recognized as several band-like structures of low and high airglow intensities. The structure was elongated from the northeast to the southwest and moved northwestward (~50° west of north) with a phase velocity of ~100 m s^{-1}. The horizontal wavelength and period of the MSTIDs were ~300 km and 50 min, respectively. Figure 2b shows temporal variation of the 630-nm airglow perturbations along the dotted line in Figure 2a, where the limb profile of the 630-nm airglow has been observed by ISUAL. The airglow perturbations with amplitude of ~30% can be seen between 132.0° and 133.5°E at ~15 UT, the observation time of ISUAL over Darwin.

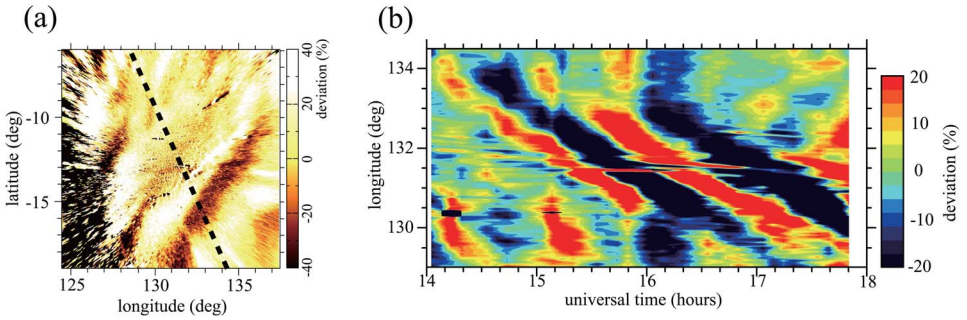

Figure 2. (a) Two-dimensional map of 630-nm airglow intensity observed with an all-sky imager at Darwin, Australia 1502 UT on May 16, 2007. A black dotted line represents the trace of the ISUAL-observed limb location. (b) Temporal variation of the 630-nm airglow perturbations along the dotted line in Figure 2a between 1400 and 1800 UT. Note that contamination by the Milky Way (Galaxy) can be identified as the striated structures at 131–132°E.

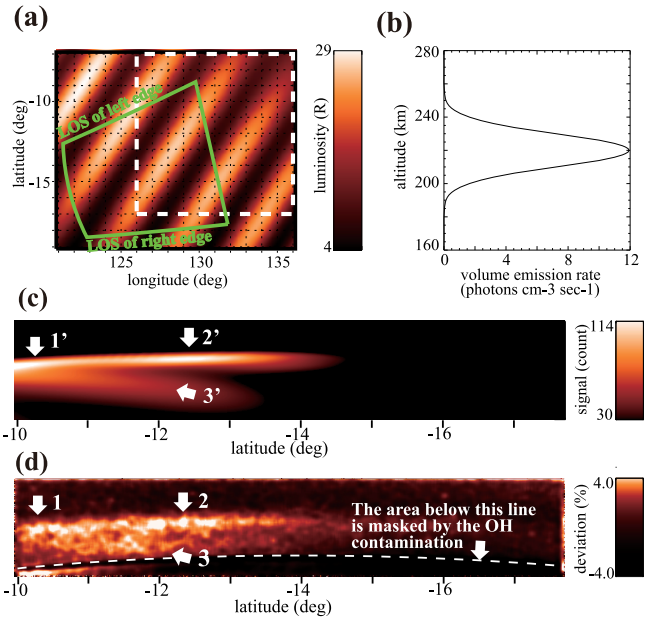

Figure 3. (a) Horizontal distributions of the 630-nm airglow assumed based on the observed structure of the MSTID shown in Figure 2a. Green solid and white dashed lines represent the fields-of-view of ISUAL (at the time of Figure 3d) and all-sky imager, respectively. (b) Vertical distribution of the airglow estimated from the ISUAL limb image with an assumption of Gaussian distribution [*Adachi et al.*, 2010]. (c) Modeled image derived by converting the assumed airglow into the ISUAL observation geometry. Due to the camera sensitivity, signal levels of the airglow emission in the right half are significantly low. (d) ISUAL-observed image.

[6] In order to compare the airglow structures obtained by both instruments, the MSTID observed by the all-sky imager was modeled with a simple sinusoidal expression and was converted into the ISUAL geometry. Figure 3a shows horizontal distributions of the modeled MSTIDs expressed by the following equations.

$$I(\alpha,\beta) = 10(1+\cos\theta)\cos\varphi + 0.5(\beta+27.5) \quad (1)$$

$$\theta = 2\pi(-(\alpha-\alpha_0)/\tan\sigma + \beta - \beta_0)\sin\sigma/L \quad (2)$$

$$\varphi = 2\pi((\beta-\beta_0)/\tan\sigma + \alpha - \alpha_0)\sin\sigma/W \quad (3)$$

[7] The parameters α and β are the geographical longitude and latitude, respectively, and $\sigma = 40°$ is the clockwise angle from the north to the direction of wave fronts. Based on the results shown in Figure 2a, the location of the maximum intensity (α_0, β_0) and the wavelength W were determined to (130.5°E, 16.0°S) and 300 km, respectively. While the typical length of the wavefronts of MSTIDs has not yet been uncovered, recent wide TEC observations reported that wavefronts could be longer than 2000 km [*Tsugawa et al.*, 2007]. In this study, the length of wavefront L was assumed as ~2500 km. The first term on the right side of equation (1) represents the perturbation due to MSTIDs while the second term represents the base airglow emissions. As found in the ISUAL latitudinal scans [*Adachi et al.*, 2010], the base emission was set to increase 100% as latitude increases from 17.5°S to 7.5°S. Figure 3b shows a vertical distribution of the airglow estimated from the ISUAL limb images. Figure 3c shows the modeled ISUAL image derived by converting the assumed airglow (Figures 3a and 3b) into the satellite observation geometry. Figure 3d shows the image observed by ISUAL. In Figure 3c, several characteristic structures due to the MSTID are found: two limb enhancements (arrows 1′ and 2′) and one horizontal structure (arrows 3′). The structures 1′–3′ clearly agree well with the structure 1–3 in Figure 3d, suggesting a consistency between the ISUAL and all-sky imager data.

[8] Further comparisons were made in Figure 4. A black line represents the ISUAL data while a gray line represents the all-sky imager data. The ISUAL data were derived by projecting successive images onto a surface of 220 km and integrating optical emissions along the orientation of wavefront. The baselines (0% level) of these data are shifted with respect to each other for the purpose of a clear illustration. In the ISUAL data, three wave structures peaking at ~130.4°E, ~132.0°E, and ~134.0°E (arrows 1–3) can be found. Similarly, airglow perturbations observed by the all-sky imager also had three peaks at ~130.5°E, ~132.2°E, and ~133.8°E (arrows 1′–3′), showing a nearly identical variation with the ISUAL data. These results strongly suggest that both instruments simultaneously observed the same airglow perturbations due to the MSTID.

3. Discussion

[9] Based on the results shown in Figures 1–4, we conclude that ISUAL succeeded in detecting an MSTID from space, which is the first space-borne imaging observation of this phenomenon. Considering that ISUAL is primarily designed for observations of bright phenomena such as lightning and TLEs, it is expected that, by developing a

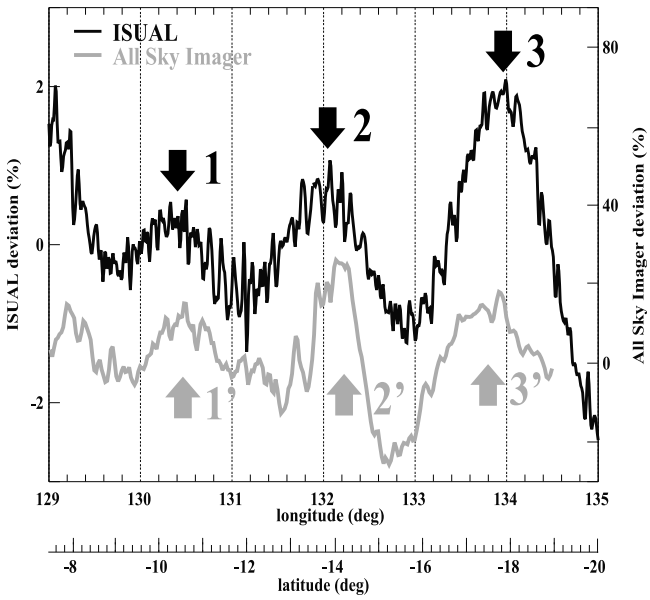

Figure 4. Perturbations of the 630-nm airglow observed by ISUAL (black) and the all-sky imager (gray) along the dotted line in Figure 2a.

lower-noise higher-sensitivity camera optimized for airglows, satellite limb observations could be a new effective tool to survey the global characteristics of MSTIDs.

[10] In the case of limb measurement, observation geometry is a sensitive issue. In Figure 4, the amplitude of the airglow perturbation observed by the all-sky imager was 20–30 percent while that observed by ISUAL was several percent. As discussed earlier, the line-of-sight (LOS) of ISUAL was not precisely aligned with the wavefronts of MSTIDs. This directional discrepancy made the ISUAL-observed structure ambiguous and the amplitude of perturbation was decreased down to a few percent levels. In order to minimize the geometrical effect, LOS needs to be aligned with the orientation of MSTIDs. Although the pass length through the airglow layer is as long as ~1000 km (see Figure 3a), this scale is still shorter than the length of wavefronts (>2000 km) estimated by a recent wide TEC observation [*Tsugawa et al.*, 2007]. Therefore, in an LOS-aligned geometry, the pass length would not play a significant role in decreasing the observed amplitude of airglow perturbation. Past studies have found that the orientation of MSTIDs varies largely between hemispheres [e.g., *Otsuka et al.*, 2004]: northeast-southwest at the southern midlatitude and northwest-southeast at the northern midlatitude. In order to observe the structures of MSTID in an ideal geometry, multi-camera observation covering northeast and southeast (or northwest and southwest) directions would be, for example, useful. In such a case, the observed amplitudes of the airglow perturbations are expected to be comparable to those observed from the ground (tens of percent). Considering that the intensity of the limb-integrated airglow layer was 200–400 Rayleigh [*Adachi et al.*, 2010], the perturbations of tens of percent correspond to 40–100 Rayleigh fluctuations, which is an observable amplitude range. Because the phase velocity of MSTIDs is sufficiently lower than the motion of a low-orbit satellite, the position of the airglow structure does not change while the satellite observes a certain location. Therefore, such structures, which can be considered to be fixed to the geographical coordinate, would be distinguishable from instrumental noise using successive satellite images as shown in Figure 1.

[11] Although past theoretical and observational studies have uncovered the fundamental electrodynamics of MSTIDs at midlatitudes, little is known about their behavior at higher and lower latitude ranges. For example, while MSTIDs at midlatitudes are known to propagate toward the equator, only a few studies have observed their behavior at low latitudes [e.g., *Makela et al.*, 2010]. Furthermore, recent studies have found banded structures of the 630-nm airglow which were nearly symmetrical between two conjugate points and suggested the role of interhemispheric coupling in producing MSTIDs [e.g., *Otsuka et al.*, 2004]. In order to understand the generation, propagation, and damping processes of MSTIDs, observations which cover a whole latitudinal range in both hemispheres should be carried out. The longitudinal dependence of the MSTID phenomenon is another critical issue. While the seasonal occurrence rate of MSTIDs is found to be different between the Asian and European sectors [*Kotake et al.*, 2006], the longitudinal dependence has not yet been fully understood because the observation sites in the past research were sparse in the world and concentrated primarily over land. In order to understand the electrodynamics which controls the occurrence rate of MSTIDs, observations covering a full longitudinal range regardless of land and ocean are essential. All the issues addressed here, which are critical to elucidate the physics of MSTIDs, require worldwide observations. In this regard, global survey using satellite imaging technique would play a crucial role in the near future.

4. Conclusions

[12] The ISUAL payload on board the FORMOSAT-2 satellite observed the 630-nm airglow simultaneously with a ground-based all-sky imager at Darwin, Australia. The ISUAL data showed wave-like airglow structures, which agreed well with the MSTID event observed by the all-sky imager. We concluded that ISUAL for the first time succeeded in observing an MSTID event from space. Such a satellite limb airglow observations can be utilized to clarify the spatial characteristics of MSTIDs and coupling processes in the ionosphere on a global level.

[13] **Acknowledgments.** TA is supported by JSPS under Postdoctoral Fellowships for Research Abroad. This work is supported by Grant-in-Aid for Scientific Research (11440145, 13573006, and 20244080) and on Priority Area (764) of the Ministry of Education, Culture, Sports, Science and Technology of Japan.

[14] W. K. Peterson thanks two anonymous reviewers.

References

Adachi, T., et al. (2008), Electric fields and electron energies in sprites and temporal evolutions of lightning charge moment, *J. Phys. D Appl. Phys.*, *41*, 234010, doi:10.1088/0022-3727/41/23/234010.

Adachi, T., M. Yamaoka, M. Yamamoto, Y. Otsuka, H. Liu, C.-C. Hsial, A. B. Chen, and R.-R. Hsu (2010), Midnight latitude-altitude distribution of 630-nm airglow in the Asian sector measured with FORMOSAT-2/ISUAL, *J. Geophys. Res.*, *115*, A09315, doi:10.1029/2009JA015147.

Cosgrove, R. B., and R. T. Tsunoda (2004), Instability of the *E-F* coupled nighttime midlatitude ionosphere, *J. Geophys. Res.*, *109*, A04305, doi:10.1029/2003JA010243.

Garcia, F. J., M. C. Kelley, J. J. Makela, and C.-S. Huang (2000), Airglow observations of mesoscale low-velocity traveling ionospheric disturbances at midlatitudes, *J. Geophys. Res.*, *105*, 18,407–18,415, doi:10.1029/1999JA000305.

Kotake, N., Y. Otsuka, T. Tsugawa, T. Ogawa, and A. Saito (2006), Climatological study of GPS total electron content variations caused by medium-scale traveling ionospheric disturbances, *J. Geophys. Res.*, *111*, A04306, doi:10.1029/2005JA011418.

Makela, J. J., E. S. Miller, and E. R. Talaat (2010), Nighttime medium-scale traveling ionospheric disturbances at low geomagnetic latitudes, *Geophys. Res. Lett.*, *37*, L24104, doi:10.1029/2010GL045922.

Otsuka, Y., K. Shiokawa, T. Ogawa, and P. Wilkinson (2004), Geomagnetic conjugate observations of medium-scale traveling ionospheric disturbances at midlatitude using all-sky airglow imagers, *Geophys. Res. Lett.*, *31*, L15803, doi:10.1029/2004GL020262.

Otsuka, Y., F. Onoma, K. Shiokawa, T. Ogawa, M. Yamamoto, and S. Fukao (2007), Simultaneous observations of nighttime medium-scale traveling ionospheric disturbances and E region field-aligned irregularities at midlatitude, *J. Geophys. Res.*, *112*, A06317, doi:10.1029/2005JA011548.

Park, J., H. Luhr, C. Stolle, M. Rother, K. W. Min, J.-K. Chung, Y. H. Kim, I. Michaelis, and M. Noja (2009), Magnetic signatures of medium-scale traveling ionospheric disturbances as observed by CHAMP, *J. Geophys. Res.*, *114*, A03307, doi:10.1029/2008JA013792.

Perkins, F. (1973), Spread F and ionospheric currents, *J. Geophys. Res.*, *78*, 218–226, doi:10.1029/JA078i001p00218.

Saito, A., T. Iyemori, M. Sugiura, N. C. Maynard, T. L. Aggson, L. H. Brace, M. Takeda, and M. Yamamoto (1995), Conjugate occurrence of the electric field fluctuations in the nighttime midlatitude ionosphere, *J. Geophys. Res.*, *100*, 21,439–21,451, doi:10.1029/95JA01505.

Saito, A., et al. (2001), Traveling ionospheric disturbances detected in the FRONT campaign, *Geophys. Res. Lett.*, *28*, 689–692, doi:10.1029/2000GL011884.

Shiokawa, K., Y. Katoh, M. Satoh, M. K. Ejiri, and T. Ogawa (2000), Integrating-sphere calibration of all-sky cameras for nightglow measurements, *Adv. Space Res.*, *26*, 1025–1028, doi:10.1016/S0273-1177(00)00052-1.

Shiokawa, K., Y. Otsuka, and T. Ogawa (2009), Propagation characteristics of nighttime mesospheric and thermospheric waves observed by optical mesosphere thermosphere imagers at middle and low latitudes, *Earth Planets Space*, *61*, 479–491.

Tsugawa, T., Y. Otsuka, A. J. Coster, and A. Saito (2007), Medium-scale traveling ionospheric disturbances detected with dense and wide TEC maps over North America, *Geophys. Res. Lett.*, *34*, L22101, doi:10.1029/2007GL031663.

Zhang, S. P., and G. G. Shepherd (2008), Variations of the O(^{1}S) and O(^{1}D) peak volume emission rates without direct solar effects, *Adv. Space Res.*, *42*, 939–946, doi:10.1016/j.asr.2007.09.004.

T. Adachi, Department of Electrical Engineering, Stanford University, 350 Serra Mall, Stanford, CA 94305, USA. (tadachi@stanford.edu)

A. B. Chen, Institute of Space, Astrophysical and Plasma Sciences, National Cheng Kung University, 1 University Rd., Tainan 70101, Taiwan.

R.-R. Hsu, Department of Physics, National Cheng Kung University, 1 Ta-Hsueh Rd., Tainan 70101, Taiwan.

Y. Otsuka and K. Shiokawa, Solar-Terrestrial Environment Laboratory, Nagoya University, Furo-cho, Chikusa-ku, Nagoya, Aichi 464-8601, Japan.

M. Yamamoto and M. Yamaoka, Research Institute for Sustainable Humanosphere, Kyoto University, Gokasho, Uji, Kyoto 611-0011, Japan.